Materials & Design 250 (2025) 113572

Contents lists available at ScienceDirect

Materials & Design

journal homepage: www.elsevier.com/locate/matdes

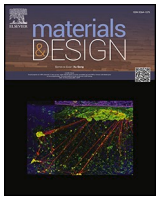

# Energy coupled to matter in additive manufacturing for controlled magnetic heterogeneity through multi-material consolidation

Malaya Prasad Behera, Yifan Lv, Sarat Singamneni *

*Additive Manufacturing Research Centre, Auckland University of Technology, Auckland, New Zealand*

ARTICLE INFO

*Keywords:*
Laser melting
Magnetic materials
External fields
Controlled magnetism
Multi-material magnets

ABSTRACT

Magnetism assisting the manufacturing process is well known within the energy coupled to matter realm and material processing assisting in the magnetic responses has also been in practice. The current research is an attempt to combine both approaches together in a multi-magnetic material consolidation process under the influence of external magnetic fields. Additive manufacturing by selective laser melting with controlled dispersion of multi-material magnetic powders and the application of controlled magnetic fields during material melting and consolidation are key features of the methodology. The melt-pool geometries, sub-granular structures, and the crystallographic orientations showed distinct responses with the use of external magnetic fields during laser consolidation of NdFeB and FeCo systems and their combinations with and without a third non-magnetic material matrix. As per the energy coupled to matter mechanisms and mechanics, the multi-magnetic material substrates consolidated by laser melting under external fields demonstrated patterned polar formations and predefined magnetic orientations. The directions and intensities of the north and south poles at different regions of the printed samples depend on the strengths and orientations of the external fields applied during consolidation and magnetisation fields employed after printing.

## 1. Introduction

Application of external magnetic fields to control material, process, structure and property relationships and responses has been in use for a while and falls under the aegis of the Energy Coupled to Matter (ECM) technological realm. ECM refers to the field assisted processing by electric, magnetic, microwave, and other fields [1]. Specifically, the use of external magnetic fields could target two specific objectives: either magnetic field assisting the manufacturing process to achieve process, structure, and property enhancements [1,2,3] or the manufacturing process assisting in enhancing the magnetic nature and responses of the products [4,5,6]. There have been methods and systems progressed in both directions.

Magnetism assisted finishing processes have seen successful implementations in the finishing of the internal surfaces of tubular structures, where conventional finishing methods and tools find it difficult to access the critical areas [7,8]. Magnetic abrasive media applied to surfaces and the abrasive tool and work relative motions achieved through external magnetic fields has been in use in surface finishing operations of complex re-entrant sections [9,10]. Use of external magnetic fields for the effective disposal of debris from the electrode region in electric discharge machining (EDM) is well known [11,12]. Higher energy densities and lower magnetic fields were shown to give the best material removal rates due to better disposal of the highly accumulated debris [13]. Higher magnetic field intensities also lower the material removal rate as the Lorenz forces affect the trajectory of the ion inflow paths.

Based on the magnetic field assisted ECM methods with high temperature processing of metals under external magnetic fields, both mechanical properties and phase transformations were shown to be controlled [14,15]. Gibbs free molar energy and associated improved bainitic transformations were demonstrated, while magnetic fields were also used to control grain alignment and crystallographic texturing [16]. Magnetic anisotropy susceptibilities amplified by doping with rare earth gadolinium and ytterbium were shown to enhance the magnetic moment localisation and magneto-crystalline anisotropy [1]. Simultaneous action of centrifugal and magnetic field forces was shown to offer additional control over the dispersion of particle chains in the centrifugal casting of ceramic slurries [17]. Competing roles between the viscous and magnetic forces were utilised in forming uniform and biphasic patterns in magnetically aligned freeze cast scaffolds [18].

* Corresponding author at:.
*E-mail address:* sarat.singamneni@aut.ac.nz (S. Singamneni).

https://doi.org/10.1016/j.matdes.2024.113572
Received 13 November 2024; Received in revised form 5 December 2024; Accepted 25 December 2024
Available online 26 December 2024

External magnetic fields are often applied during the slip and freeze casting processes to achieve structures and scaffolds of controlled porosities to control and orient the ceramic grains in preferred directions. As most ceramics are diamagnetic, strong external fields or mixing of magnetic elements into the slurry are often used to achieve better magnetic susceptibilities [18].

Controlling the magnetic responses of fabricated materials was mainly attempted by means of controlling the dispersion of magnetic particles in polymer bonded magnets under the action of external magnetic fields [19]. Chain- and sheet-like microstructural formations were achieved for the magnetic particles dispersed in a preform polymer substrate cured under the action of an external magnetic field as the dipole moments align themselves along the magnetic easy axis [20]. Magnetic susceptibility, saturation and coercivity enhance along the field direction apart from process enhancements leading to the possible control on the resulting bulk magnetic anisotropy. The current research focuses on combining both magnetism-assisted manufacturing and manufacturing-assisted magnetism together to evaluate the possibilities to achieve controlled magnetic heterogeneity in consolidated parts through additive processing of the hard magnetic NdFeB and soft magnetic FeCo by selective laser melting under external magnetic fields. There have been previous studies on the laser melting of both alloys, but with no external magnetic fields applied.

Nanocrystalline magnets made by selective laser melting a mixture of MQP-B grade NdFeB alloy (in 25 nm and 450 nm states) and (Pr0.5Nd0.5)3(Cu0.25Co0.75) eutectic alloy, were reported to exhibit $Nd_2Fe_{14}B$ along with new phases like α-Fe and (Nd, Pr)$_2O_3$, achieving a significantly higher coercivity (μ0Hc) of 1.6 T and better temperature stability compared to the initial powders possibly due to reduced inter grain exchange interactions from the paramagnetic eutectic alloy layer [21]. Single-beam laser powder bed fusion (LPBF) of NdFeB magnets based on an infrared fibre laser yielded coercivity and magnetic energy product values at 264 kA/m and 12.41 kJ/m$^3$ and with optimal parameters in continuous wave mode the same were shown to increase to 555 kA/m, and 24.91 kJ/m$^3$ respectively. Further evaluation by the three-beam method with a two-zone scanning strategy was shown to significantly improve the results, with optimal parameters achieving 521 kA/m, and 33.42 kJ/m$^3$, for the coercivity and maximum energy product responses respectively, with a density of 6.95 g/cm$^3$, while reducing the scanning time by 38 % [22].

Tosoni et al. evaluated mechanically milled NdFeB flakes with 3.7 wt % Dy and 0.96 wt% of copper for selective laser melting and achieved magnetic remanence, coercivity and maximum energy product values 0.62 T, 1790 kA/m, and 65 kJ/m$^3$ respectively further to a magnetic heat treatment process [23]. Custom made Nd9.4Pr3.2Dy1.6Fe bal (CoCuAlGa)1.7B6.0 powders were evaluated by Caniou et al. for selective laser melting, identifying different melt-pool geometries and precipitation of α-Fe and Nd2Fe17Bx phases with varying process conditions and cooling rates [24]. The as-built magnets initially had coercivity HcJ 92 ± 2 kA/m, remanence Br 0.39 ± 0.01 T, and energy product (BH)max 7.4 ± 0.2 kJ/mˆ3, which, after an optimum heat treatment, improved to HcJ 551 ± 10 kA/m, Br 0.55 ± 0.01 T, and (BH) max 38 ± 1 kJ/mˆ3. Urban et al. investigated the laser beam melting for NdFeB alloys, based on MQP-S-11–9 powder based on the Mlab Cusing R system with varying process conditions showing that optimal settings at 40–55 W laser power and 1200–2000 mm/s scanning speed can achieve high density and polarisation, particularly with meander exposure patterns [25]. While these studies clearly indicate the progress made with the evaluation of NdFeB alloys for processing by selective laser melting, significant cracking during laser consolidation due to internal stresses has been a major hurdle [26]. Optimum process conditions with the best combinations of laser power, scan speed and layer thickness, together with the appropriate choice of hatch styles, raster schemes, and heated build chamber conditions were shown to mitigate the residual stresses and associated cracking problems to a large extent, paving ways for the production complex hard magnetic components based on selective laser melting of NdFeB alloys [27,28,29].

With the best combination of high permeability, low coercivity, and high saturation magnetism attributes, the equi-atomic Fe-Co alloys are good for soft magnetic applications. However, the ordered intermetallic B2 phase reduces the dislocation mobility, rendering them to be brittle and difficult to process by conventional means. Considering the dependence of the transformation from the parent disordered BCC phase to the ordered B2 phase on the rate of cooling in the solid state, the rapid cooling rates typical of the additive consolidation methods attracted research attention as a possible means of effectively processing FeCo alloys on the recent past. It was shown that the rapid melting and solidification and associated thermal variations result in high dislocation densities and disordered BCC phase in equi-atomic FeCo alloys processed by selective laser melting [30]. Additive manufacturing of FeCo alloys by the direct energy deposition (DED) method was shown to offer better magnetostrictive responses compared to the rolled counterparts [31]. Selective laser melted FeCo specimens were investigated establishing the structure vs mechanical property relationships and the evolving microstructures with varying geometrical and process conditions [32]. Experimental evaluation of laser melted FeCo alloy with a 2 wt% vanadium, the Hiperco® 50A alloy showed a significant loss of mechanical and magnetic properties compared to the traditionally made magnets mainly due to porosity, but the results could have been the outcome of lack of optimisation of critical experimental parameters [33]. On the other hand, Kustas et al, showed laser engineered net shaping (LENS) process as a promising method for producing bulk forms based on FeCo alloys [34].

Evidently, additive processing of NdFeB and FeCo magnetic materials has been in progress for some time and progress made to some extent. However, the possible integration of energy coupled to matter (ECM) material consolidation is not attempted yet. The current proposal is to explore this approach by the integration of external magnetic fields into the point-by-point consolidation of NdFeB and FeCo particles by the laser powder bed fusion method utilising the innovative solutions recently filed for a couple of patents by the authors. This innovation allows the use of external magnetic fields in 3D printing, leading to enhanced magnetic performance as well as the creation of complex shapes and internal cooling channels. The main objective is to explore the hypothesis that the point-by-point material consolidation typical of additive manufacturing can be effectively utilised to achieve controlled magnetic heterogeneity in printed substrates by combining both multi-material printing and the use of external magnetic fields together. Such attempts were made in the making of bonded magnets in polymer matrices by injection moulding initially [35] and through 3D printing of polymer composites by fused deposition modelling [36,37,38] and stereolithography recently [39,40].

There have been some attempts applying external magnetic fields in additive processing of metal powers too. However, these were mainly focused on controlling the microstructures and enhancing the mechanical properties of printed parts. It was realised that integrating external magnetic fields during fabrication allows for precise control over microstructures, leading to improved mechanical performance and the development of multifunctional materials. Hu et al. [41] reviewed the integration of magnetic, electric, and acoustic fields with AM technologies, highlighting that applying magnetic fields can effectively tailor microstructures and enhance mechanical properties. Al et al. [42] reported promising results through field-assisted techniques in controlling filler orientation and concentration within composites, leading to improved surface finish and microstructural properties, thereby enhancing the overall quality of the fabricated parts. Zhao et al. [43] demonstrated that a static magnetic field applied in the laser additive manufacturing of Ti6Al4V alloy results in refined microstructures, leading to enhanced mechanical properties. Research in similar lines, clearly demonstrated that the use of external magnetic fields can lead to grain refinement and texture modification, better melt pool solidification dynamics and phase distribution, and enhanced mechanical

properties in powder bed fusion, laser cladding, and wire arc additive manufacturing methods applied to different grades of steels or Inconel [44–49].

Apparently, external magnetic fields were used in the context of additive manufacturing either to achieve controlled particle distribution in polymer bonded substrates or microstructural controls in powder bed fusion of metals. The current research takes it beyond to the processing of multiple magnetic material combinations processed by selective laser melting. A multi-material processing approach by selective laser melting is attempted simultaneously consolidating two or three different magnetic materials the hard NdFeB and the soft FeCo alloys with or without a non-magnetic material into a common substrate. The experimental research aims to prove that the point-by-point consolidation of multi-material powder bed arrangement integrated with externally applied magnetic fields allows to control the magnetic nature and the orientation of the easy axes from one point to the other programmatically. This will pave ways to the complex realm of controlled magnetic heterogeneity. The outcomes are positive, as multi-material magnetic substrates were successfully produced with controlled directions of the magnetic easy axes.

## 2. Materials and methods

Spherical powder particles of relatively homogeneous sizes at around 30 μm produced by gas atomisation are the most common forms of raw materials used for selective laser melting. The spherical and similarly sized particle morphologies presumably promote better dispersion of the powder on the build platform. However, with hard magnetic material options such as NdFeB, gas atomised powder feedstock is very expensive due to the presence of the rare earth element. It is observed that if the dispersion aspects are reasonably dealt with, the particle shapes do not actually affect the powder consolidation in the later stages as the laser heating would completely melt and fuse these particles into continuous layers. Caniou *et. al* have shown sufficient powder dispersion qualities and subsequent consolidation by laser melting while experimenting with irregular particles of NdFeB alloys produced by jet milling strip-cast ribbons under nitrogen atmosphere [24]. Considering these aspects, custom made irregularly shaped NdFeB particles, produced by

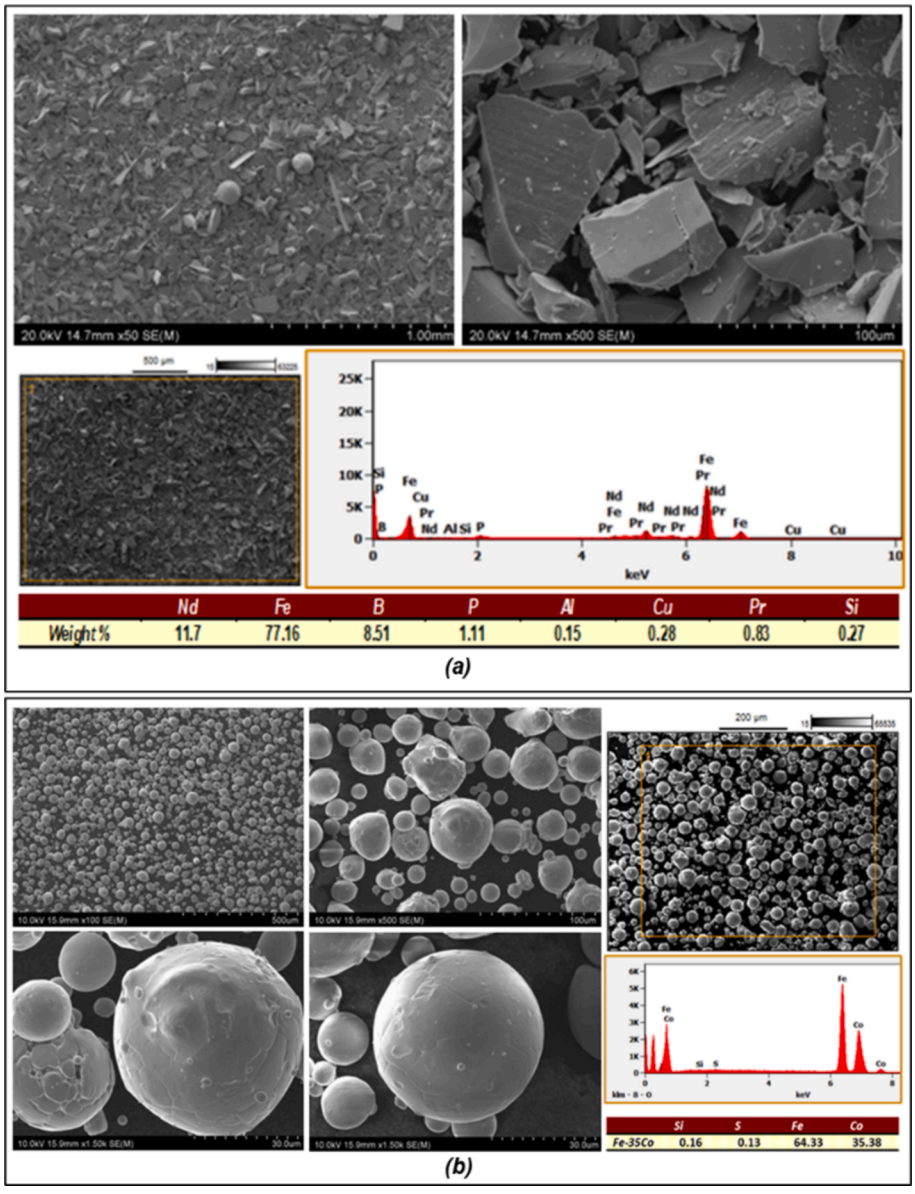


**Fig. 1. SEM images and the elemental mapping based on EDS analysis** of the (a) mechanically ground NdFeB powder feedstock with irregular flake-like and (b) gas atomised Fe35Co powder feedstock with spherical morphologies.

mechanical grinding and pulverisation by Luoyang Tongrun Info Technology Ltd, China are employed in all the current trials.

SEM images of the irregular NdFeB powder particles used as the key magnetic raw materials are presented in Fig. 1 (a). The irregular flake-like particle morphology is typical of the mechanical grinding method used to pulverise the raw material castings into the powder form. Widespread variation in the particles size is also evident, but if these particles can slide easily under the silicone embedded wiper blade during the powder dispersion stage, the variation in the particle size actually helps in the heating, initiation and spreading of the melt pools and the final consolidation into solid layers. The smaller particles will pick up the heat first and melt fully, enclosing the rest of the bigger flakes, which will then either completely or partially be melted and assimilated into the wider melt-pool, depending on the energy densities applied during laser consolidation. EDS analysis indicates the composition of the magnetic material to be Nd 11.7 %, Fe 77.16 %, B 8.51 %, P 1.11 %, Al 0.15 %, Cu0.28 %, Pr 0.83 %, and Si 0.27 % by weight.

Both FeSi and Fe35Co alloys were evaluated as the options for the soft magnetic material phase but considering the ease of working and the better laser melting responses, finally converged on the Fe35Co system. Considering the ready availability as off-the-shelf options, gas atomised Fe35Co powders are procured again from Luoyang Tongrun Info Technology Ltd, China. SEM images of the Fe35Co powder particles are presented in Fig. 1(b) and the EDS elemental mapping ascertains the composition to be Fe 64.33 % and Co 35.38 % by weight, with minor traces of silicon and sulphur. Before attempting to include both soft and hard magnetic material options in a single printed part, it is also necessary to first evaluate a magnetic and a non-magnetic material option to go together on a common printed part. This non– magnetic material should have a compatibility with the magnetic option to be included within its matrix. After a preliminary search and a few laser melting trials, the high entropy alloy (HEA) option based on the FeCo combination which is totally non-magnetic and proved to be suitable for laser additive manufacturing is converged on. Gas atomised powders of HEA based on FeCo is procured from the same source with the composition Fe 20.11 %, Co 20.15 %, Cr 18.8 %, Mn 21.99 % and Ni 18.95 % by weight and is used as the matrix non-magnetic material with inclusion of NdFeB islands under controlled external magnetic fields.

All the selective laser melting trials are conducted based on the Renishaw AM400 system at the Additive Manufacturing Research Centre of the Auckland University of Technology (AUT). The system is equipped with a solid state Nd:YAG laser system with a 1070 μm wave length and 70 μm spot size. Cubic samples are produced with parallel raster paths aligned in the same direction and perpendicular to the direction of spreading the powders by the wiper blade. Generally, meander style, with a $67^0$ rotation of the parallel scan lines in alternative layers is used for a more uniform consolidation of the powder substrates in SLM. However, in this case, considering the focus on the fundamental understanding of the influence of external magnetic fields on the consolidation mechanics of the magnetic materials, the simplest raster scheme is used for establishing the interactions between the process conditions and responses of materials consolidated with and without external magnetic fields. All the samples are printed directly on the build plate without any support structures and then removed from the build plate by wire EDM, without causing any thermal or mechanical damages to the internal structures. The MAKINO U3 CNC Wire EDM system is used for this purpose with a zinc coated brass wire of 0.25 mm diameter and deionised water as the di-electric fluid.

Magnetic specimens produced are sectioned also by wire-EDM and polished without mounting using polishing papers of increasing grit numbers in the order P80, P500, P1200, and P2400, on the polishing system METASERV, removing the oxides, scaling and other contaminants. This is followed by the final polishing step with 6 μm and then 1 μm diamond paste using the Struers LaboPol-2 setup, before etching by 3 % Nital, for micro-examinations. For the optical microscopy and imaging the Olympus BX51 digital optical microscope is used and scanning electron microscopy evaluations are done using the Hitachi SU-70 Schottky field emission system. Samples used for EBSD mapping are electropolished using the 590 ml ethanol plus 330 ml butoxyethanol plus 78 ml perchloric acid solution as electrolyte using the Struers Lectropol-5 system for 90 s at 20 V and 5 $^0$C. EBSD maps are generated using an EDAX detector on the SEM operated at 20 kV accelerating voltage, 13.5 mm working distance and a step size of 200 nm and interpreted by the Thermo Scientific NORAN System 7 (NSS) version 3.3.113 software. Low angle and high angle grain boundaries are defined with misorientation angles between $2^0$-$15^0$ highlighted in grey colour and more than $15^0$ highlighted in black, respectively.

The printed samples are magnetised in different orientations using a high voltage capacitive magnetiser Model DXMM-20C70 with operational voltage range from 0 to 1870 V and maximum magnetic field intensity 3.5 T procured from Xiamen Dexing Magnet Tech. Co. Ltd, China. Magnetic domain mapping is attempted based on the Magvision Kerr System available at the Robinson Institute, Victoria University of Wellington though the experiments are not fully successful as the solid metallic samples vibrate and move under the applied field even after sling to the thinnest possible sections and polished. Alternatively, the Bitter Pattern imaging technique is used to capture the magnetic domain wall images, where a thin colloidal suspension of nano magnetic particles is painted on polished specimens and the resulting distribution patterns are captured by optical microscopy [50]. Heterogeneous magnetic nature of the printed specimens are captured by the magnetic probe measurements using a hand-held Gauss meter model DX-102 supplied by Dexing Magnet Ltd. The printed specimens removed from the build plate are first polished and a grid pattern is drawn on the polished surface. The magnetic probe is used to record the magnetic intensity levels and polarities at all the grid points. The point cloud data thus gathered is used to plot the magnetic intensity contours using a linear interpolation scheme coded in MATLAB.

The build plate of the laser melting system is modified to include multiple electromagnets placed at different locations as needed and controlled from an external circuit based on an invention by the authors, the full patent application of which is currently submitted. A detailed drawing of one of the several embodiments included in the patent application is presented in Fig. 2 (a) as an example. This particular design is a schematic representation of a single static electro-magnetic element inserted into the build-plate along with a control system to be integrated with the selective laser melting scheme. Working models of this embodiment with one, two, and four electro-magnetic assemblies were fabricated and employed in the overall scheme of the research, but in the current context, the arrangement with only two magnets is employed. The multi-material test pieces printed are rectangular slabs of 10 mm X 10 mm X 1 mm dimensions as depicted in the CAD model of Fig. 2 (b). The magnetic cage under the build pate has two electromagnets located at the two ends of the printed slab as shown in Fig. 2 (c). it may be noted that the magnetic field direction on the left is North upwards, while the one on the right side is North downwards. This arrangement is commonly used together with the specially designed powder dispensing system to build thin rectangular samples of *i)* NdFeB islands placed non-magnetic high entropy FeCoMnNiCr alloy matrix, *ii)* NdFeB islands placed in soft magnetic FeCo alloy matrix and *iii)* FeCo islands embedded into the NdFeB matrix by selective laser melting under external magnetic fields.

It may be noted that the application of the magnetic field will have an influence on the dispersion and orientation of the magnetic particles over the powder bed. However, in the current case, the magnetic field is always perpendicular to the face of the build plate and the powder bed surface. This will always align the magnetic particles along the build direction, whether the field is north upwards or *vice versa*. It is also pertinent to point out that it is only the magnetic particle phase that is aligned with the magnetic field while the non-magnetic counterpart particles remain undisturbed within the multi-material powder bed substrate. There will be some conglomeration of the magnetic particles

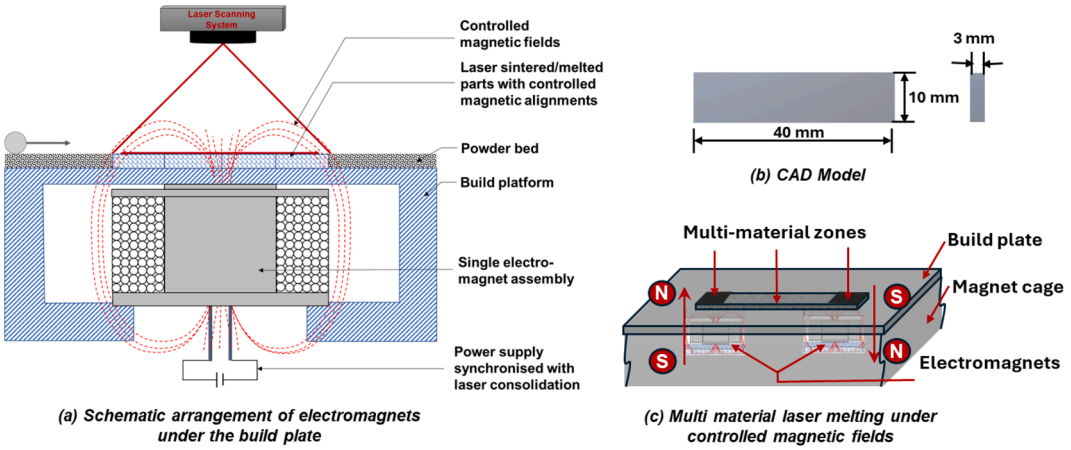


**Fig. 2. Powder bed fusion under external magnetic field** (a) schematic arrangement for the application of external electromagnetic field based on a modified build plate accommodating the electromagnetic assembly, (b) CAD model of the specimens printed, and (c) The multi-material consolidation of magnetic powders under external fields.

around the external magnetic field pattern. However, once the laser strikes, the powder layer melts and the magnetic influence will be temporarily switched off as the melt pool regions go beyond the Curie Temperature. This will eliminate any localised magnetic particle distribution patterns due to the use of external fields during the powder dispersion stages.

## 3. Results

### 3.1. Initial laser melting trials and best process conditions

Consolidation of NdFeB powders by selective laser melting though reported earlier [21,22,23,24,25,26], is challenging as the process window is quite narrow. Furthermore, the density of consolidation has always been lower, given the precarious nature of point-wise consolidation and the final printed parts will end up with significant porosity, as was the case in the literature reported earlier, even when using the gas atomised spherical powder feedstock [21,22,23,24,25,26]. With the flaky irregular particle powder feedstock currently used, identifying the process window became even more involving. A series of laser melting tests were done in different sets as per the process parameter combinations as listed in Table 1. The line energy or the energy density levels arising out of these process combinations are also listed in Table 1. Both Set I and Set II trials involving the maximum and minimum energy levels respectively, failed to achieve sufficient consolidation of the cubic samples. Laser melting trials with the parameter combinations listed in Set II and IV with lower and upper medium levels of line energy respectively gave better consolidation results. The cubic samples built as per the conditions of Set II and IV are presented in Fig. 3 (a) and (b) respectively, while Fig. 3 (c) is a close-up view at some of the samples built as per the conditions in Set IV. It may also be noted that some of the trials in Set IV with a laser re-melting at different levels of energy reductions from the initial pass did not improve the consolidation and finally ended up as failed components. Based on the physical observations of the quality of these cubic samples, the process parameter combinations with laser power/scan speed at 100 W/300 mm/s, 120 W/400 mm/s, and 140 W/500 mm/s are identified to be the best for further experimental evaluations.

A detailed characterisation of the resulting microstructures is not the focus of this current paper but evaluation of the indicative optical microscopy images obtained with the NdFeB samples laser melted with different process and raster conditions elucidated the shape and size of the melt-pool boundaries to vary significantly, but in accordance with the process conditions. Photomicrographs obtained based on the sample produced with laser power 140 W and scan speed 500 mm/s taken on cross sections along and perpendicular to the laser scan lines are

**Table 1**
Laser power and scan speed combinations evaluated at different stages, progressing from one set to the other, together with the resulting line energy or energy density values.

| SET I | | | | SET III | | | | |
|---|---|---|---|---|---|---|---|---|
| *Laser Power (W)* | *Scan speed (mm/sec)* | | | *Laser Power (W)* | *Scan speed (mm/sec)* | | | |
| | *150* | *200* | *250* | | *400* | *500* | *600* | *700* |
| | Line energy (J/mm) | | | | Line energy (J/mm) | | | |
| | | | | *60* | 0.150 | 0.120 | 0.100 | 0.086 |
| *75* | 0.500 | 0.375 | 0.300 | *80* | 0.200 | 0.160 | 0.133 | 0.114 |
| *100* | 0.667 | 0.500 | 0.400 | *100* | 0.250 | 0.200 | 0.167 | 0.143 |
| *125* | 0.833 | 0.625 | 0.500 | *120* | 0.300 | 0.240 | 0.200 | 0.171 |

| SET II | | | | | | | SET IV | | | |
|---|---|---|---|---|---|---|---|---|---|---|
| *Laser Power (W)* | *Scan speed (mm/sec)* | | | | | | *Laser Power (W)* | *Scan speed (mm/sec)* | | |
| | *600* | *700* | *800* | *900* | *1000* | *1100* | | *300* | *400* | *500* |
| | Line energy (J/mm) | | | | | | | Line energy (J/mm) | | |
| *30* | 0.050 | 0.043 | 0.038 | 0.033 | 0.030 | 0.027 | *100* | 0.333 | 0.250 | 0.200 |
| *40* | 0.067 | 0.057 | 0.050 | 0.044 | 0.040 | 0.036 | *120* | 0.400 | 0.300 | 0.240 |
| *50* | 0.083 | 0.071 | 0.063 | 0.056 | 0.050 | 0.045 | *140* | 0.467 | 0.350 | 0.280 |
| | | | | | | | *100* | $2^{nd}$*100 W* | $2^{nd}$*50 W* | $2^{nd}$*25 W* |
| | | | | | | | *Remelting layer* | *Failed* | *Failed* | *Failed* |

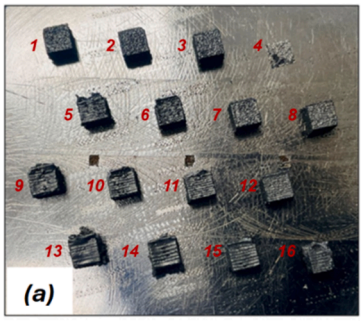


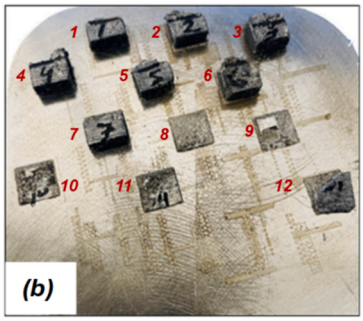


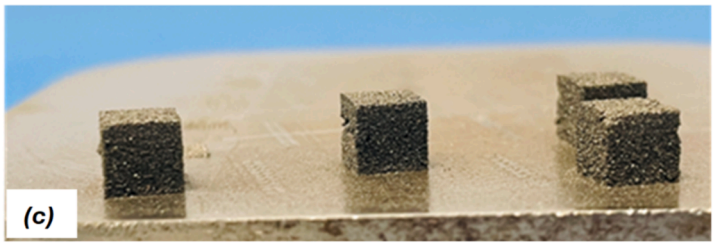


| SET III | | | | |
|---|---|---|---|---|
| Laser Power (W) | Scan speed (mm/sec) | | | |
| | 400 | 500 | 600 | 700 |
| 60 | 1 | 2 | 3 | 4 |
| 80 | 5 | 6 | 7 | 8 |
| 100 | 9 | 10 | 11 | 12 |
| 120 | 13 | 14 | 15 | 16 |

| SET IV | | | |
|---|---|---|---|
| Laser Power (W) | Scan speed (mm/sec) | | |
| | 300 | 400 | 500 |
| 100 | 1 | 2 | 3 |
| 120 | 4 | 5 | 6 |
| 140 | 7 | 8 | 9 |
| 100 | 10 | 11 | 12 |
| Remelting layer | Failed | Failed | Failed |

**Fig. 3. Photographic images of the cubic samples built as per the process conditions** (a) Set III and (b) Set IV listed in Table 1 and with sample numbers marked, and (c) close-up view at some of the samples of Set IV.

presented in Fig. 4 (i) (a) and (b) respectively for further observations. The deeply etched samples show granulated dark zones at the liquid pool boundaries with a characteristic directional dendritic growth, the extent of which depends on the raster orientations. The molten pool geometry is uniform, with half-moon shaped troughs as evident in Fig. 4 (i) (a) and like the results reported with similar alloys and process conditions earlier [22]. Porosity is also evident in the sample as dark spherical dots spread across the microstructure, but the consolidation in this case is far better compared to the continuous grid-like cracks observed in laser melted NdFeB alloys earlier by Caniou et al [24]. The dark areas all along the melt-pool boundaries represent the dendritic growth of the soft magnetic Fe phase, segregating first due to the non-equilibrium cooling rates at the far boundaries and growing in a direction opposite to the heat flow. Along with this, columnar growth of NdFeB grains are also seen as white patches of varying sizes and extent. The central regions of the melt-pool are typically equiaxed grains of around 1 μm size of the magnetic phase NdFeB of varying compositions depending on the colour reflection, from light grey to white areas [26]. Similar observations can be made from Fig. 4 (i) (b) where the strands show the layers laid out one over the other.

Unlike the NdFeB powder in the flaky form, the FeCo powders used are gas atomised spherical particles of suitable sizes and standard forms as evaluated earlier by others and reported in the literature. As a result, the process evaluation and parametric optimisation could be completed with relative ease and converge on the best possible laser power and scan speed as 220 W and 780 mm/s respectively with a layer thickness of 40 μm and hatch distance 70 μm. Optical microscopy images of laser melted FeCo samples parallel and perpendicular to the scan directions are presented in Fig. 4. (ii) (a) and (b) respectively, displaying the characteristic single-phase ordered α2-FeCo solid solution. The epitaxial growth of the long columnar grains is clearly evident in Fig. 4 (ii) (b), looking at a cross section perpendicular to the scan direction. Other images obtained based on samples made at $45^0$-raster orientation indicated a widening of these epitaxial columnar grains growing across multiple layers, and the meander option resulted in an intermediate grain structure due to the rotating scan directions from one layer to the other.

### 3.2. *Selective laser melting under external magnetic fields*

It is pertinent now to turn the attention to the role of external magnetic fields applied during the laser consolidation of these two alloys. For this, the experimental setup patented by the authors and the schematic representation of which, for one of the embodiments is as depicted in Fig. 2 (c) is used. Essentially, electromagnets are placed under a modified build platform and controlled to turn the magnetic

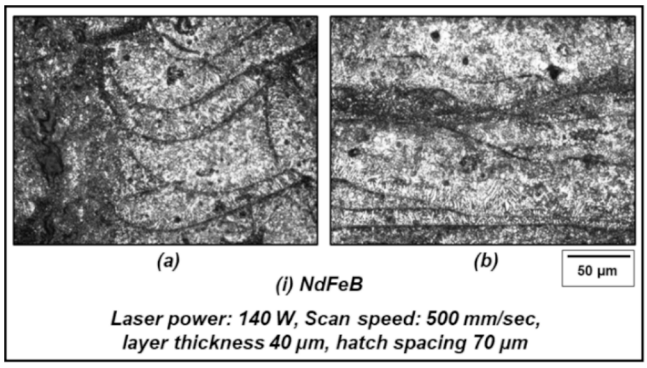


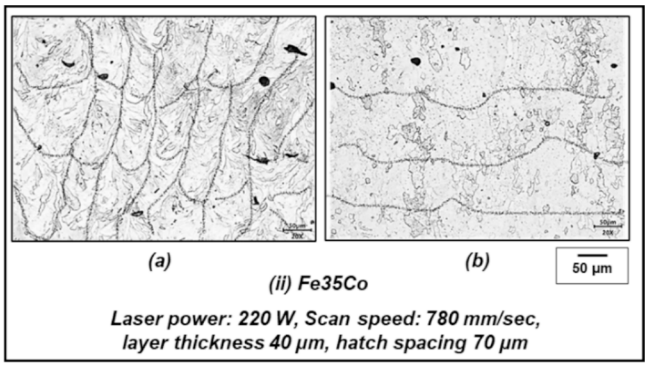


**Fig. 4. Optical microscopy images of the polished and etched specimen produced** (i) using NdFeB with laser power 140 W and scan speed 500 mm/s (a) perpendicular and (b) parallel to the laser scan direction (ii) using Fe35Co with power 220 W, scan speed 780 mm/s, layer thickness 40 μm, hatch spacing 70 μm (a) perpendicular and (b) parallel to the laser scan direction.

field 'ON' and 'OFF' as needed during the laser scanning and solidification process. Optical microscopy images of NdFeB samples produced under the same laser power (140 W) and scan speed (500 mm/s) without and with the use of external magnetic fields are shown in Fig. 5 (i) (a) and (b) respectively for observing the differences in the material consolidation mechanics.

For the same magnification, a quick comparison of the two images in Fig. 5 (i) elucidates that the half-moon shaped wider and shallow melt-pool geometries in the case of the sample produced without any external magnetic field as in Fig. 5 (i) (a) has been visibly changed to a deeply drawn and narrowed down topology as in Fig. 5 (i) (b), with the application of the magnetic field. After dispersing the powder on the bed and as the magnets are turned 'ON', each powder particle gets magnetised, assuming the dipole configuration, under the influence of the external magnetic field. Before the laser striking the powder bed, the polarised magnetic particles are aligned in the direction of flux lines of the external magnetic field. A localised particle pattern also results on the powder bed in accordance with the external magnetic field dispersion. Once the laser strikes the powder bed, the thermal conditions quickly change and go beyond the Curie temperature. Once this happens, the magnetic field applied will have no influence on the molten pool. However, due to the rapid movement of the laser point, these changes take place quite rapidly and once the melt pool starts cooling down, which is also in a rapid mode, the magnetic field begins to have its role on the melt pool again. As already stated in the materials and methods section, the external field aligned in the build direction will not affect the magnetic particle dispersion in the lateral directions (parallel to the build surface). However, there will be some agglomeration of the magnetic particles around the external field patterns, along with a vertical build up particles in the build direction. Subsequent laser heating and melting beyond the Curie temperature will temporarily turn the magnetic nature of the powder particles off, relaxing all the preferential dispersion patterns due to the external field. This will bring the multi-material powder dispersion almost to the normal expected patterns in selective laser melting without causing any significant variations in layer thickness due to powder movement and aggregation.

Due to the rapid loss of heat to the substrate layers, the lower boundaries of the molten pools experience more rapid cooling and will quickly go below the Curie temperature. This brings the magnetic nature of the material back to life within the thin narrow zones all around the melt pool boundaries and more so at the lower limits of the troughs. The external magnetic field will try to drag this towards the build plate at this stage. These drag forces together with the dynamic nature of the rest of the melt pool being still in liquid state results in the deeply drawn topologies for the melt pools, which will finally solidify in those shapes. A closer look at the microstructures indicate subtle changes between the two cases. The Fe-rich dendritic growth at the melt pool boundaries noted in the case of the sample normally are reduced drastically in the case with external magnetic fields. Also, the NdFeB grains formed within the central regions of the melt pools are more refined and uniformly dispersed all around.

Similar observations as above can also be noted comparing the two micrographs in Fig. 5 (ii) (a) and (b) of laser melted Fe35Co samples without and with the use of external magnetic fields. Further, electron back scatter diffraction (EBSD) results obtained based on the laser melted Fe-Co samples produced without and with the use of external magnetic fields are presented in Fig. 6 (a) and (b) respectively. Based on the direction of minimum magneto-crystalline anisotropic energy principle, either $< 100 >$ or $< 111 >$ are the preferred directions for magnetisation in ferromagnetic materials. The magnetic domain configurations will depend on this energy. As seen in Fig. 6 (a), the crystal orientation is predominantly in the $< 101 >$ direction when there is no external magnetic field influencing the solidification process. For the same process conditions, the application of the external magnetic field led to a more intricate and fine granular structure as evident in the pattern quality image on the left of Fig. 6 (b). Further, the BCC normal EBSD image in Fig. 6 (b) indicates a variation of the crystal orientations from $< 001 >$ to $< 101 >$, and $< 111 >$ across different grains. The effect of the external magnetic field in influencing the solidification process to progress in differential crystallographic directions is evident from these results.

Magnetic domain mapping of the printed samples was attempted using the magneto-optic Kerr effect (MOKE) microscope at the Robinson Institute, Victoria University Wellington, New Zealand. MOKE microscopy uses polarised light reflecting from the magnetised surface to build images of the magnetic domains, based on the changes in the intensities of the light passing through the polarisation filter of the analyser. MOKE measurements were done on several test pieces produced with varying compositions, process, and raster geometries, with practical difficulties, as the solid (despite being sliced and polished to thin sections of 1 mm thickness) samples move when the magnetic field is strong enough to change the magnetisation. Experience suggests that MOKE microscopy is by far used to mapping magnetic domains in thin films, where the force is too low to move the sample. The relatively more solid specimens in this case made it difficult to focus properly on the samples for measurements with in-plane fields.

With a redesigned and 3D printed rib structure added to the sample mounting system allowed some success with the MOKE microscope and to establish the structure vs magnetic domain relationships. Typical results with the Fe-Co sample produced at the $45^0$-raster orientation without and with the use of external magnetic fields are shown in Fig. 6 (c) and (d) respectively. A quick examination of these results clearly

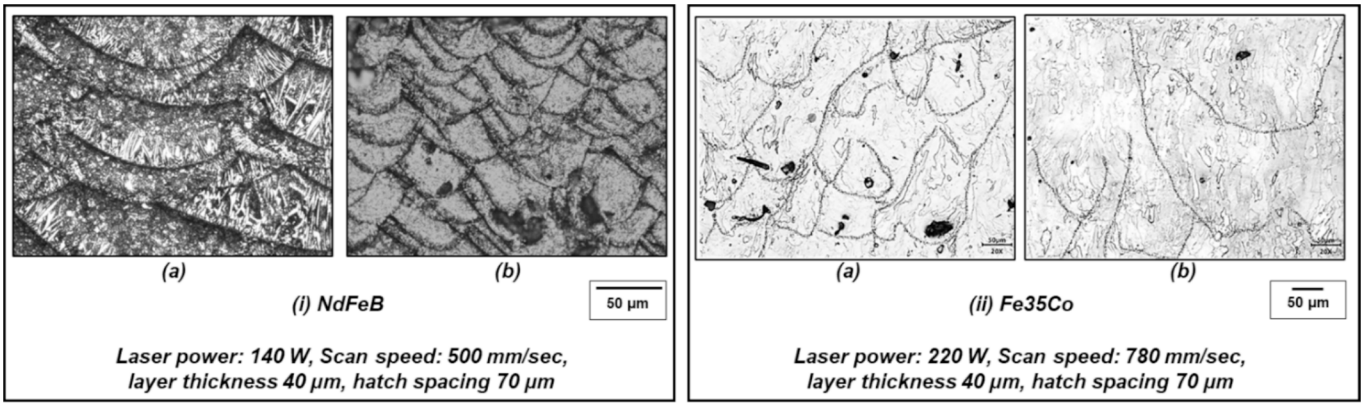


**Fig. 5. Optical microscopy images of the polished and etched specimen produced** (i) NdFeB samples laser melted with laser power 140 W, scan speed 500 mm/s and $0^0$ parallel raster plans across all layers (a) without and (b) with the application of external magnetic fields, and (ii) Fe35Co samples laser melted with power 220 W, scan speed 780 mm/s, layer thickness 40 µm, hatch spacing 70 µm (a) without and (b) with the application of external magnetic fields.

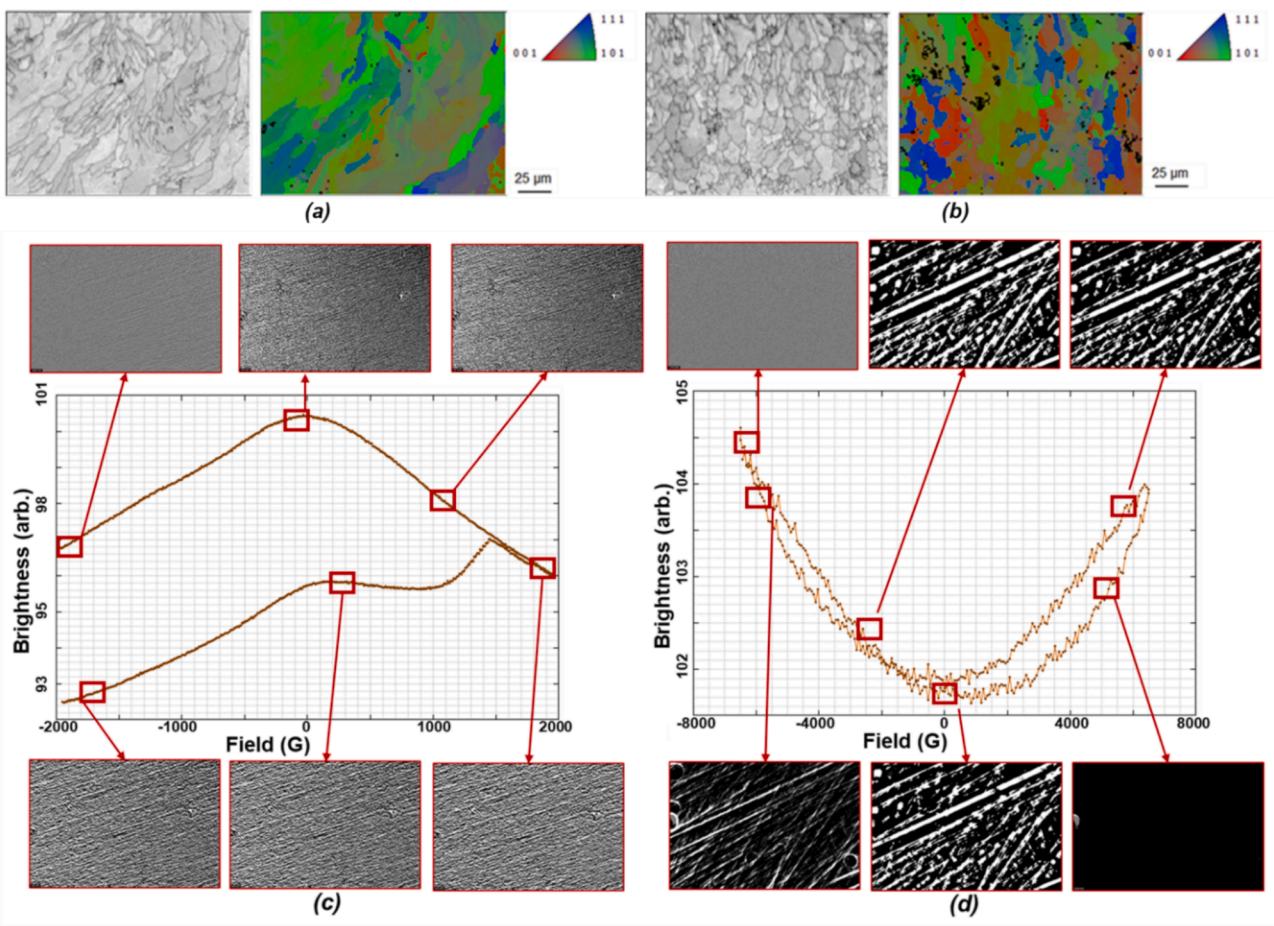


**Fig. 6. EBSD mapping of Fe35Co samples laser melted** (a) without and (b) with external magnetic fields. Magnetic domain mapping based on the MOKE microscopy measurements using FeCo specimen laser melted with 220 W power, 780 mm/s scan speed, 70 μm hatch spacing, 40 μm layer thickness and $45^0$ raster orientation (c) without the use of external magnetic fields and (d) with the use of external magnetic fields.

indicates the magnetic domain structures deviating to a more widely spread white areas with thick dark borders in the case of the sample produced under the influence of external magnetic fields (Fig. 6 (d)), aligning with the microstructural patterns observed in the optical microscopy and the EBSD results based on SEM analysis.

### 3.3. Controlled magnetic heterogeneity

Once the role of the external magnetic field on the material consolidation mechanics of laser melted magnetic materials is established, the next and more intriguing target of the current research is exploring the control magnetic heterogeneity in substrates printed under controlled magnetic fields. This means consolidation of functionally graded magnetic materials based on powder bed fusion through selective laser melting. Practically, this has proved to be the most challenging part in this work as achieving the controlled dispersion of different magnetic materials is quite involving on the build plate, below which, the electromagnetic components are already retrofitted. A novel solution is developed and implemented which has led to a provisional patent application currently filed by the authors. While the IP protection process is still in progress, this specially developed device can be retrofitted into the build chamber of the selective laser melting system and achieve controlled dispersion of different magnetic material powders for laser consolidation into multi-polar substrates with controlled magnetic variations.

With the controlled dispersion of multiple magnetic powders on the build plate achieved, different laser scan parameters as are apt to different zones are applied by considering the areas occupied by the constituent materials as multiple parts in each layer, consolidated by the laser scan scheme. This has allowed easy integration of the multi-material powder bed consolidation into the commercial software interface which otherwise assumes a single material powder bed. Samples produced by selective laser melting hard magnetic NdFeB segregated into specific locations in a non-magnetic FeCoMnNiCr material, soft magnetic FeCo matrix, and FeCo segregated selectively into the NdFeB matrix are shown in Fig. 7 (a), (b), and (c) respectively. Evaluation of the controlled magnetic heterogeneity across the domain of a physical printed part is based on measuring the macroscopic variation of magnetic flux values over a large area relative to the ranges of MOKE microscopy or the bulk magnetic hysteresis measurements. As a result, the magnetic probe method is used to record the magnetic strength values at several pre-selected points on the top face of each of the printed slab. Fig. 7 (d) shows the schematic of a grid pattern used to mark a set of points on the top face of each of these multi-material and multi-polar magnetic substrates for measuring the magnetic field responses and plotting the *iso*-magnetic flux lines.

The data collected by the magnetic probe manually from each grid point is transferred into a spread sheet to process in MATLAB and construct the *iso*-magnetic field intensity lines. The first case to be examined is the sample produced with the non-magnetic high entropy FeCoMnNiCr alloy as the matrix and the hard magnetic NdFeB concentrated towards the ends of the rectangular specimen of dimensions as described in the methods section. The *iso*-magnetic field strength lines generated on this sample when it is still attached to the build plate, just after removing from the build plate, after magnetising in a 1.4 T field along the preferred easy axis and then magnetising in a

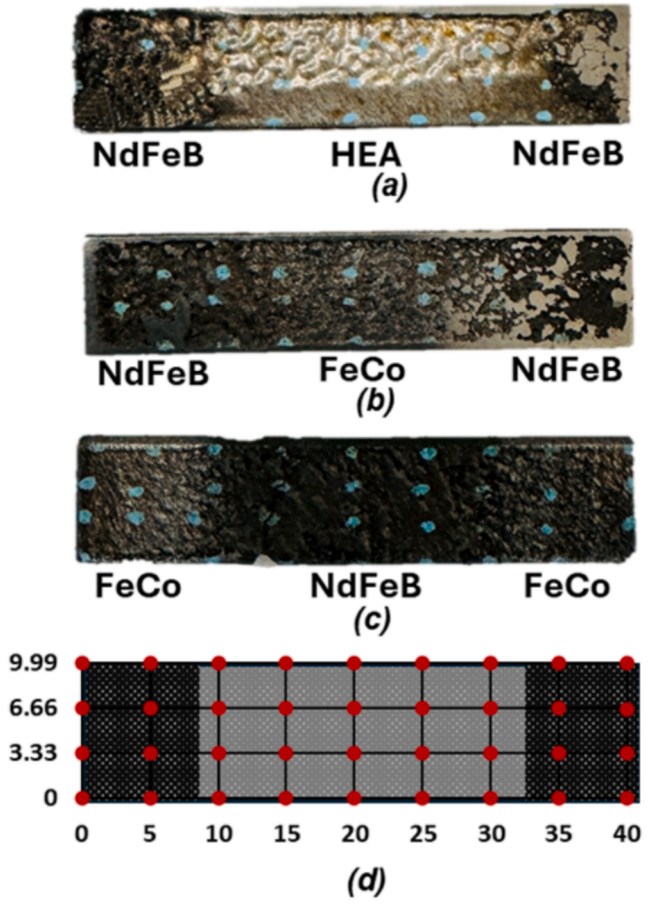


**Fig. 7. Multi-material consolidation by laser powder bed fusion integrated with external magnetic fields to produce components with controlled magnetic material dispersion, field responses, and polarities by laser melting** (a) NdFeB in a non-magnetic FeCoMnNiCr matrix, (b) NdFeB in a soft magnetic FeCo matrix, (c) soft magnetic FeCo in hard magnetic NdFeB matrix, and (d) the schematic of the grid points used for the Gauss-probe measurements of magnetic flux responses.

reverse magnetic field of 3.5 T are presented in Fig. 8 (a), (b), (c), and (d) respectively.

The magnetic field intensity results probing the top surface of the printed part when it is still attached to the build plate as seen in Fig. 8 (a) are mild but generally indicative of a north pole towards the right and a south pole towards the left for the NdFeB islands created within the non-magnetic FeCoMnNiCr high entropy alloy matrix, as imposed by the external magnetic fields applied on either end during laser consolidation. This response is more clearly indicative in the *iso*-magnetic field contours of Fig. 8 (b) from the printed part after it is removed from the build plate. It may also be noted in Fig. 8 (c) that after magnetising this samples in an external field along the direction of the inherent magnetic easy axis (North upwards) led to the maximum magnetic field intensity at the north pole on the right side to reach 30 mT, while at the predominantly south pole towards the left edge, the effect of this external field is negligibly small. In fact, there is a slight tendency for the left edge to turn towards being a north pole. The central regions made of the non-magnetic high entropy alloy are totally non-receptive to any of these changes, remaining neutral to the external magnetic fields. These results prove two important hypotheses that are the basis for this work: that i) the unique point-wise material consolidation mechanics typical of selective laser melting can be extended to build multi-material magnetic components and ii) the direction and nature of the external magnetic fields applied at different locations during consolidation can be used to effectively control the directional polarities of different regions of the sample. Further, the reverse polarity at the highest level 3.5 T led to a change of polarity from North to South on the right edge, but clearly to a milder extent, reaching a maximum of 15 mT as in Fig. 8 (d), which is further evidence that the specimen produced has a preferred magnetic orientation as dictated by the mechanics of materials consolidation under the closely controlled external fields.

Similar *iso*-magnetic field lines obtained examining the specimen laser melted embedding hard magnetic NdFeB islands within the soft magnetic FeCo matrix are presented in Fig. 9 (a) to (d). This is a more complex arrangement of the dual magnetic material dispersion within the same block of the printed substrate and as a result, the magnetic field responses are also quite mixed. The contours obtained before removing the printed slab from the build plate already show the magnetic polar distributions as expected, as indicated by the north pole on the right at 2 mT and the south pole on the left at 2 mT in Fig. 9 (a). Once the test piece is removed from the build plate, the magnetic field distribution has changed to horizontal orientation, with a north–south dual polar arrangement in the two halves of the top surface as seen in Fig. 9 (b). The presence of the soft magnetic matrix in the central regions has led to this variation in the magnetic field response as the hard magnetic NdFeB zones with remnant magnetic field also have magnetised the central regions.

Once the sample is magnetised under a 1.4 T north upward field, a more dramatic shift in the magnetic field dispersion resulted from the distributed dual phase magnetic materials in the specimen. The *iso*-magnetic field contours of Fig. 9 (c) show a south upward and north downward split at either ends of the bar with the field lines symmetrically dispersed around the central regions. The remanent magnetism at either end has reached an equal 50 mT at both the north and south polar regions. The central regions show no magnetic nature as the soft magnetic FeCo phase loses magnetism once the external field is removed. The vertical orientation of the magnetic fields of the NdFeB islands at the two ends are localised and not spreading into the central zones and so the soft FeCo region mostly remained with no remnant magnetism.

With the specimen subjected to a reverse magnetic field at 3.5 T, the north and south poles are flipped almost symmetrically, at the two ends as evident in Fig. 9 (d). Further, the maximum field strength at both pole regions at the two ends has been reduced almost to half of that observed in Fig. 9 (c). Even though the strength of the reverse field applied for the result in Fig. 9 (d) is more than double the field applied to obtain the result in Fig. 9 (c), the lesser magnetic strength attained is due to the preferential orientation of the magnetic easy axes along the build direction, substantiated by the application of the external magnetic field during the multi-material consolidation by laser melting. The Bitter pattern image obtained from this sample as presented in Fig. 9 (e) clearly elucidates the magnetic domain patterns as per the field contours in Fig. 9 (c) and (d), which is physical evidence of the validity of the *iso*-magnetic field contours obtained and the patterned polar responses of the substrates.

The magnetic field line responses based on the specimen produced with soft-magnetic FeCo islands within NdFeB matrix are presented in Fig. 10 at different stages. There is almost negligible magnetic response in the as built stage and still attached to the build plate, as reflected in Fig. 10 (a). After removal from the build plate, the sample has shown a predominantly south pole region in all the central NdFeB portions of the top face, while the north pole goes to the other side of the specimen, though with a minor magnetic remanence as evident in Fig. 10 (b). Once the sample is magnetised in a north upward field of 1.4 T, the south and north orientation of the central zones still remains the same, but the maximum magnetic remanence has increased to 50 mT and 30 mT in the north and south pole regions of the central NdFeB regions as seen in Fig. 10 (c). The orientation of these magnetic polar regions and the extent to which they spread are all dependent on the dispersion of the dual magnetic phases used in consolidating the test piece. When treated in the reverse magnetic field at 3.5 T, the specimen broke into pieces as

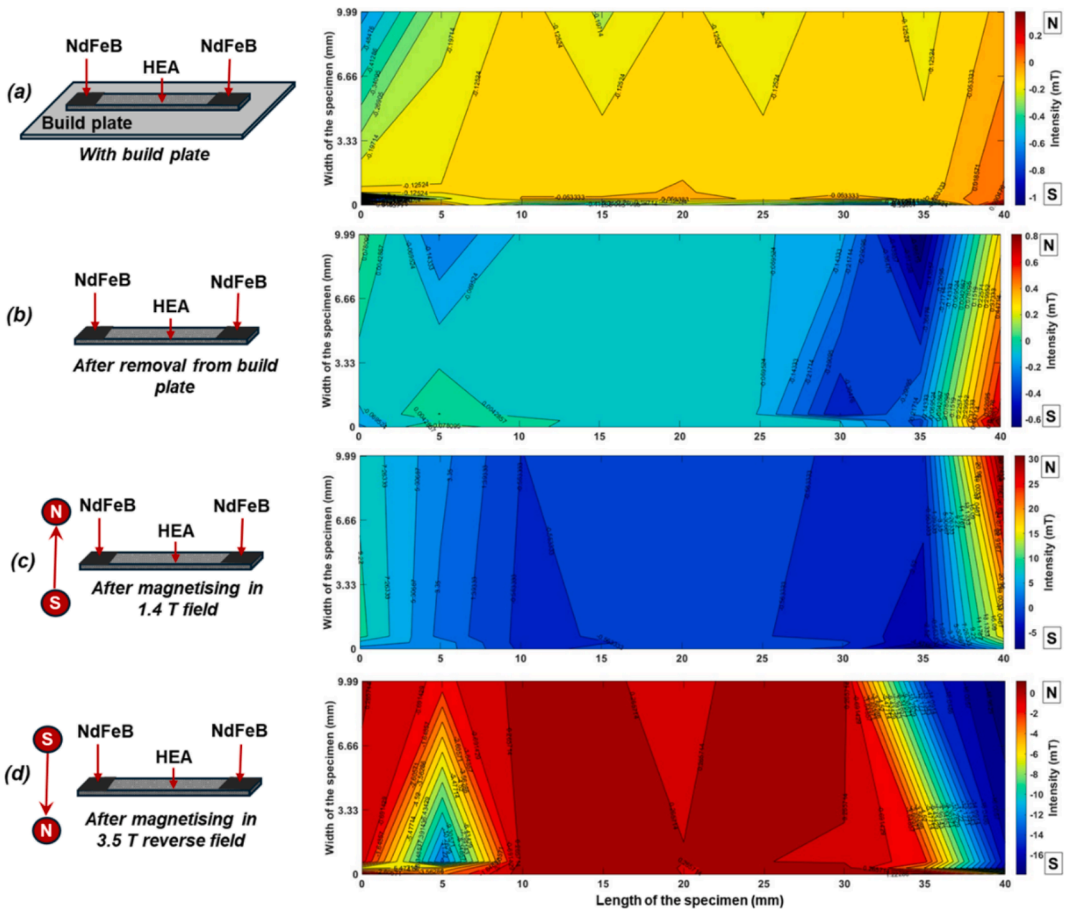


**Fig. 8. Iso-magnetic field lines obtained from the Gauss-probe measurements on the top surface of the sample produced with controlled placement of NdFeB islands at the two ends within the matrix of a non-magnetic high entropy FeCo alloy under external magnetic fields** (a) before the printed part is removed from the build plate, (b) after removing from the build plate, (c) after magnetising in a 1.4 T field applied in a North upward direction and (d) after magnetising in a reverse field of 3.5 T in a North downward direction.

shown in Fig. 10 (d), due to excessive magnetostrictive forces between the opposing fields in the soft and hard magnetic regions.

## 4. Discussion

In general, gas atomised powders of spherical morphologies with uniform dimensions at around 30 to 40 μm are used for selective laser melting, given the powder dispersion and compacting requirements. In the current case, the NdFeB raw material used is in the mechanically ground flaky form. The dispersion of these flakes was found to be reasonable on the powder bed, but the laser consolidation led to unwanted porosity as the variations in the sizes of the flakes make it difficult to apply the best processing conditions out of the already narrow window of laser melting opportunity with this alloy. Under the best possible processing conditions, the finer flakes may receive higher energy densities than needed and release absorbed gases due to overheating, while the larger flakes may suffer from lack of fusion due to insufficient energy input. After establishing the most promising process parameter conditions for selective laser melting of mechanically ground hard magnetic NdFeB flakes and gas atomised soft magnetic FeCo powders, two intriguing aspects were explored in the current research: i) controlled dispersion and laser processing of both soft and hard magnetic materials and non-magnetic materials together into a common consolidated part and ii) the application of controlled external magnetic fields during the laser consolidation of these multi-material magnetic zones.

A careful consideration of the results elucidated both approaches to be promising. Considering the role of the external magnetic field on the laser melting of the candidate materials individually, both NdFeB and FeCo responded to the external field as evident from the microstructures. The melt pool geometries in NdFeB appear to be drawn downwards probably due to the field force pulling the initial solid phases segregating all along the boundaries and cooling down below the Curie temperature, where the magnetic nature returns. The rest of the melt pool being in the liquid or mushy stage still, the field forces are able to stretch the solidifying boundary zones downward. EBSD results based on the FeCo system, also revealed that the microstructures turned into a more intricate and fine granular structure under the action of external magnetic field during melting and solidification. The crystal orientations also changed from a predominantly $< 101 >$ to an equal variation from $< 001 >$ to $< 101 >$ and then $< 111 >$ in different crystals that are finely distributed all around in the central regions of the melt pools. MOKE microscopy studies displayed distinctly different magnetic domain images based on samples produced with and without the use of external magnetic fields.

The raw magnetic particles dispersed on the powder bed in each layer will assume vertical alignment configurations with the application of the external magnetic field. However, as the laser strikes the powder bed and the temperature of the melting and fusing powder particles goes beyond the Curie temperature, the external field effects will be nullified. At this stage, the melt pool topology and dynamics are free of the field effects. However, the microstructural observations of Figs. 5 and 6 indicate variations specific to the external fields. Evidently, the solidified melt pool geometries and the ensuing structural variations have

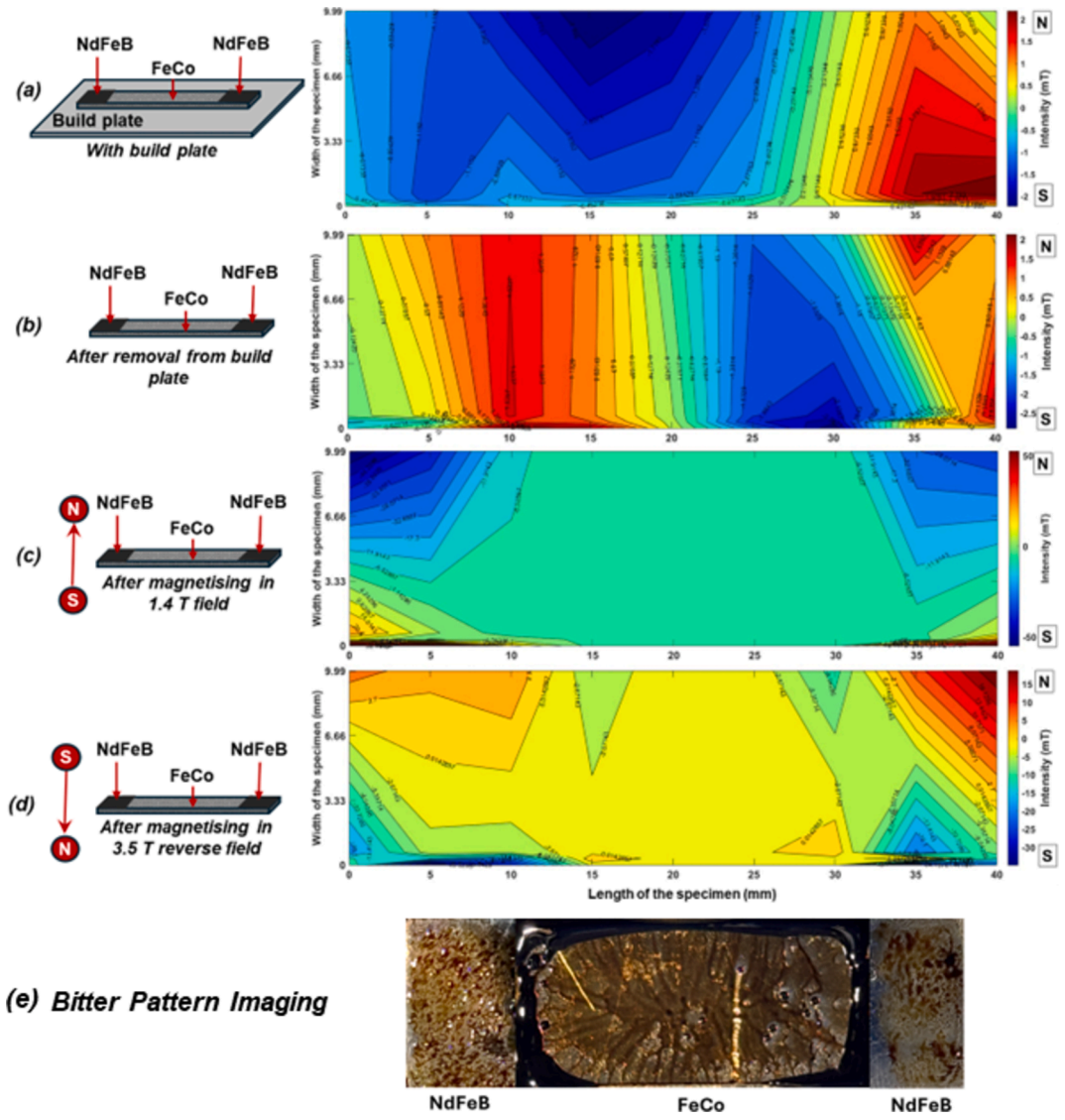


**Fig. 9. Magnetic field responses of the samples produced with controlled placement of hard magnetic NdFeB islands at the two ends within the matrix of a soft magnetic FeCo alloy under external magnetic fields** (a) before the printed part is removed from the build plate, (b) after removing from the build plate, (c) after magnetising in a 1.4 T field applied in a North upward direction and (d) after magnetising in a reverse field of 3.5 T in a North downward direction and (e) Bitter pattern image under a mild magnetic field.

been influenced by the field after the substrate returns to the magnetic temperature range. It may also be possible that the pre-melting magnetisation of the individual particles already has an influence on the nature of each of these particles which will possibly trigger the structural differentiations attributed to the substrates consolidated under the influence of the external fields.

Combined consolidation of NdFeB islands segregated into non-magnetic FeCoMnNiCr, soft magnetic FeCo matrices and FeCo islands in NdFeB matrix is demonstrated to be achievable to significant density levels by multi-material laser melting with controlled variation of process parameters across each layer and under external magnetic fields. All these three cases have shown magnetic field contours as per the polarities imposed by the external magnetic fields, though mildly, in the as built states on the build plate and immediately after removal from it. Magnetisation of the samples removed from the build plate has also clearly elucidated the controlled orientation of the magnetic easy axes achieved by means of the external magnetic fields applied during laser melting and solidification. Magnetisation in alignment with the anticipated direction of the magnetic easy axes demonstrated high magnetic intensities and concentrated polar regions while the results are mild and even reversed to some extent when magnetising in the opposing directions with varying field strengths. The multi-material magnetic substrates produced by laser melting under external magnetic fields demonstrated preferred magnetic orientations as per the energy coupled to matter mechanisms and mechanics.

The fact that the magnetic substrates consolidated under the influence of the external magnetic field have demonstrated preferred directions for the magnetic easy axes adds strength to the earlier argument that the external field has an influence on the structure and magnetic nature of the laser consolidated substrate. Presumably, the early magnetisation of the particles and their alignment along the field direction before the interaction with the laser induce specific magnetic properties and responses, aligning the crystal structures and the ensuing magnetic easy axes in preferential directions. Once the laser melting and consolidation is completed, the influence of the prior magnetic field orientation remains frozen in the solidified substrate and strongly resists reorientation even with the application of flipped magnetic fields of higher order.

Multiple materials and controlled magnetic heterogeneity also leave traces of magnetic exchange coupling effects and patterned magnetic

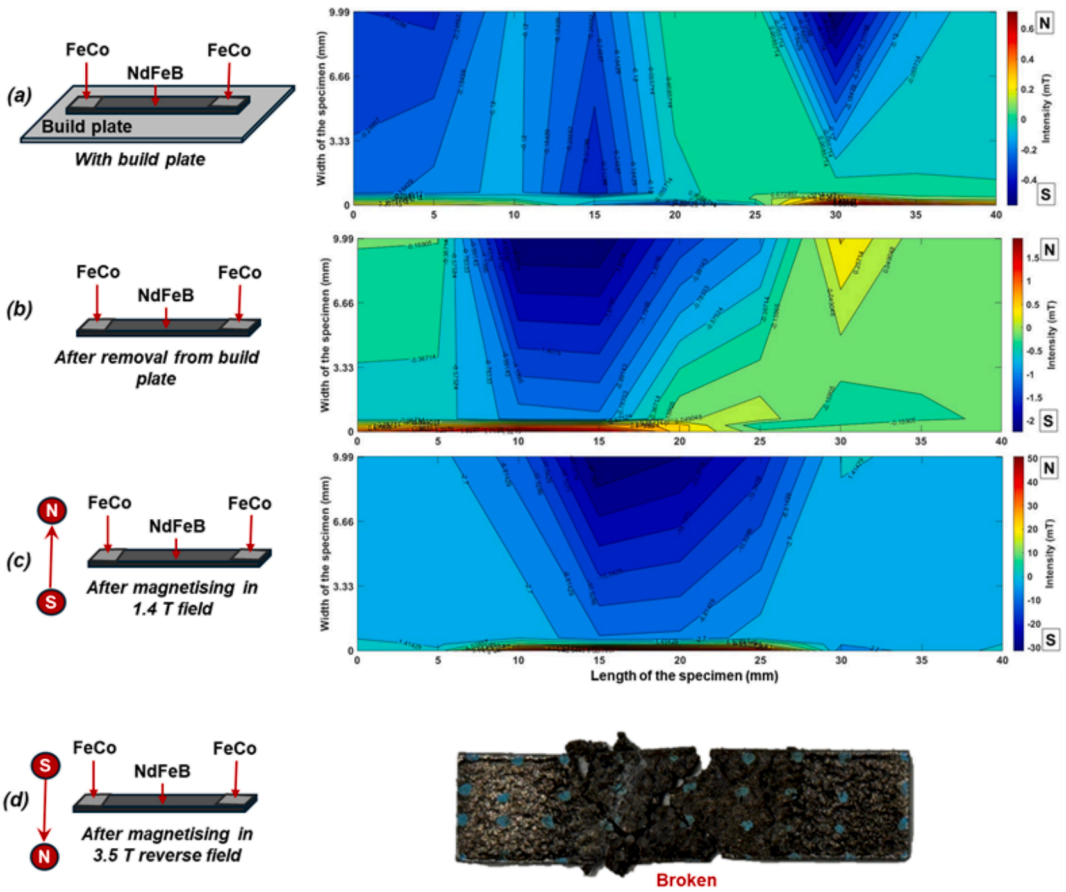


**Fig. 10. Magnetic field lines on the top surface of the samples produced with controlled placement of soft magnetic FeCo islands at the two ends within the matrix of a hard magnetic NdFeB alloy under external magnetic fields** (a) before the printed part is removed from the build plate, (b) after removing from the build plate, (c) after magnetising in a 1.4 T field applied in a North upward direction and (d) after magnetising in a reverse field of 3.5 T in a North downward direction.

pole formations. The consolidation of hard and soft magnetic materials within non-magnetic matrices showed considerable strength and density of consolidation at the multi-material interfaces with the use of compatible high entropy alloys such as the FeCoMnNiCr used in this case. However, with the hard and soft magnetic materials consolidated into different regions, without the buffer zones in between, excessive magnetostrictive forces resulting from the patterned polar regions could cause brittle fractures propagating along the boundaries between regions of opposing polarities. Overall, the laser melting and magnetic characterisation results from the current work proved the overarching hypothesis of this research that controlled material consolidation with the use of external magnetic fields in powder bed fusion technologies can lead to components with tailored magnetic responses and preferential directions for the magnetic easy axes. From the literature we came across so far, this is the first time such magnetic components with controlled variation of materials from soft to hard magnetic in nature are produced by laser melting under the influence of external magnetic fields.

## 5. Conclusion

The current research supports the hypothesis that controlled magnetic heterogeneity is possible in multi-material magnetic substrates consolidated by selective laser melting under the influence of external magnetic fields. Controlled dispersion of multiple magnetic materials on the powder bed and combined consolidation of the same with varying laser melting conditions layer-by-layer were demonstrated successfully. External magnetic fields were integrated into the selective laser melting of multi-material powder beds influencing the magnetic material consolidation mechanics. Together, the energy coupled to matter additive manufacturing of multiple magnetic materials led to controlled magnetic responses both by the varying material phases and the effects of the external fields applied. The interfaces between NdFeB and FeCoMnNiCr high entropy alloy and hard magnetic NdFeB and soft magnetic FeCo combinations showed sufficient powder consolidation. Both structural and magnetic responses were influenced by the material and external magnetic field conditions. The findings elucidate that the direction of the magnetic easy axes could be controlled by the direction of the external fields applied during the laser melting stages. The following are some of the quantitative inferences drawn from the experimental results:

- EBSD results indicate that the crystal orientation changes from $< 001 >$ to $< 101 >$ and $< 111 >$ with the use of external magnetic fields in laser meted FeCo soft magnetic powders.
- The samples produced with NdFeB islands within the high entropy alloy matrix resulted in a maximum north pole field of 0.2 mT, 0.8 mT, and 30 mT on the top surface while on the build plate, immediately after removing from the build plate, and after magnetising in a favourable external field at 1.4 T respectively
- The same sample resulted in a zero- northward polarity on the top surface once the external magnetic field was flipped at 3.5 T.
- The samples produced with NdFeB islands within the FeCo alloy matrix resulted in a maximum north pole field of 2 mT, 2 mT, and 50 mT on the top surface while on the build plate, immediately after

removing from the build plate, and after magnetising in a favourable external field at 1.4 T respectively

- The same sample as above resulted in a 15 mT northward polarity on the top surface once the external magnetic field was flipped at 3.5 T.
- The samples produced with FeCo islands within the NdFeB alloy matrix resulted in a maximum north pole field of 0.6 mT, 1.5 mT, and 50 mT on the top surface while on the build plate, immediately after removing from the build plate, and after magnetising in a favourable external field at 1.4 T respectively.

## Author contributions

Professor Sarat Singamneni is the recipient of the Marsden Funding from the Royal Society of New Zealand which supported this research and played a central role in conceptualization, methodology, resources, writing original draft, reviewing and editing, supervision, and project administration. Dr Malaya Prasad Behera the postdoctoral research fellow on the Marsden Fund and facilitated all investigation, methodology, validation, visualisation, and writing and editing of original drafts. Dr Yifan Lv is another post-Doctoral Research Fellow at AUT and contributed to the writing, reviewing and editing of the manuscript, apart from some help with the investigation.

## CRediT authorship contribution statement

**Malaya Prasad Behera:** Writing – original draft, Resources, Methodology, Investigation, Conceptualization. **Yifan Lv:** Writing – review & editing, Writing – original draft, Methodology, Investigation, Conceptualization. **Sarat Singamneni:** Writing – review & editing, Writing – original draft, Supervision, Resources, Project administration, Methodology, Funding acquisition, Conceptualization.

## Declaration of competing interest

The authors declare the following financial interests/personal relationships which may be considered as potential competing interests: Sarat Singamneni reports financial support was provided by Royal Society of Arts NZ. If there are other authors, they declare that they have no known competing financial interests or personal relationships that could have appeared to influence the work reported in this paper.

## Acknowledgements

The authors wish to acknowledge the support received by the Marsden Fund Grant No. MFP AUT1901 from the Royal Society of New Zealand Te Apārangi in carrying out the research reported in this paper.

## Appendix A. Supplementary data

Supplementary data to this article can be found online at https://doi.org/10.1016/j.matdes.2024.113572.

## Data availability

Data will be made available on request.

## References

[1] R. Brennan, et al., Energy coupled to matter for magnetic alignment of rare earth–doped alumina, Mater. Manuf. Process. 33 (1) (2018) 93–98.
[2] J. Zygmuntowicz, et al., The Structural and Mechanical Properties of Al2O3–Ni Composites Obtained by Magnetic Field-Assisted Centrifugal Slip Casting, Materials 17 (2024) 16.
[3] P. Niksiar, et al., Microstructural evolution of paramagnetic materials by magnetic freeze casting, J. Mater. Res. Technol. 8 (2) (2019) 2247–2254.
[4] H. Song, J. Spencer, A. Jander, J. Nielsen, J. Stasiak, V. Kasperchik, P. Dhagat, Inkjet printing of magnetic materials with aligned anisotropy, J. Appl. Phys. 115 (17) (2014) 17E308.
[5] D. Kokkinis, M. Schaffner, A.R. Studart, Multimaterial magnetically assisted 3D printing of composite materials, Nat. Commun. 6 (1) (2015) 8643.
[6] Y. Kim, et al., Printing ferromagnetic domains for untethered fast-transforming soft materials, Nature 558 (7709) (2018) 274–279.
[7] Y. Wang, Hu. Dejin, Study on the inner surface finishing of tubing by magnetic abrasive finishing, Int J Mach Tool Manu 45 (1) (2005) 43–49.
[8] H. Yamaguchi, T. Shinmura, Internal finishing process for alumina ceramic components by a magnetic field assisted finishing process, Precis. Eng. 28 (2) (2004) 135–142.
[9] G.-W. Chang, B.-H. Yan, R.-T. Hsu, Study on cylindrical magnetic abrasive finishing using unbonded magnetic abrasives, Int J Mach Tool Manu 42 (5) (2002) 575–583.
[10] J.-D. Kim, Polishing of Ultra-clean Inner Surfaces Using Magnetic Force, Int. J. Adv. Manuf. Technol. 21 (2003) 2.
[11] Y.-C. Lin, H.-S. Lee, Machining characteristics of magnetic force-assisted EDM, Int J Mach Tool Manu 48 (11) (2008) 1179–1186.
[12] Y.-C. Lin, et al., Optimization of machining parameters in magnetic force assisted EDM based on Taguchi method, J. Mater. Process. Technol. 209 (7) (2009) 3374–3383.
[13] R. Teimouri, H. Baseri, Effects of magnetic field and rotary tool on EDM performance, J. Manuf. Process. 14 (3) (2012) 316–322.
[14] G.M. Ludtka, G. Mackiewicz-Ludtka, G.D. Pfaffmann, Advanced induction heating coupled with magnetic field processing, Ind. Heat 81 (2013) 43–48.
[15] P. Gillon, Uses of intense dc magnetic fields in materials processing, Mater. Sci. Eng. A 287 (2) (2000) 146–152.
[16] R.A. Jaramillo, et al., Effect of 30 T magnetic field on transformations in a novel bainitic steel, Scr. Mater. 52 (6) (2005) 461–466.
[17] J. Zygmuntowicz, et al., Investigation on fabrication and property of graded composites obtained via centrifugal casting in the magnetic field, Compos. B Eng. 173 (2019) 106999.
[18] I. Nelson, S.E. Naleway, Intrinsic and extrinsic control of freeze casting, J. Mater. Res. Technol. 8 (2) (2019) 2372–2385.
[19] S. Safaee, et al., Field-assisted additive manufacturing of polymeric composites, Addit. Manuf. 51 (2022) 102642.
[20] J.E. Martin, et al., Anisotropic magnetism in field-structured composites, Phys. Rev. E 61 (3) (2000) 2818.
[21] A.S. Volegov, S.V. Andreev, N.V. Selezneva, I.A. Ryzhikhin, N.V. Kudrevatykh, L. Mädler, I.V. Okulov, Additive manufacturing of heavy rare earth free high-coercivity permanent magnets, Acta Mater. 188 (2020) 733–739.
[22] K.-S. Yu, et al., Additive manufacturing of NdFeB magnets by synchronized three-beam laser powder bed fusion, Opt. Laser Technol. 146 (2022) 107604.
[23] O. Tosoni, et al., High-coercivity copper-rich Nd-Fe-B magnets by powder bed fusion using laser beam method, Addit. Manuf. 64 (2023) 103426.
[24] R. Caniou, et al., Influence of process parameters on the microstructure of laser printed NdFeB alloys, J. Magn. Magn. Mater. 570 (2023) 170503.
[25] N. Urban, F. Huber, J. Franke, Influences of process parameters on rare earth magnets produced by laser beam melting. 2017 7th International Electric Drives Production Conference (EDPC), 2017.
[26] N. Emminghaus, et al., Laser Powder Bed Fusion of NdFeB and influence of heat treatment on microstructure and crack development, Procedia CIRP 94 (2020) 211–216.
[27] K. Genç, et al., Laser powder bed fusion of NdFeB and influence of powder bed heating on density and magnetic properties, Int. J. Adv. Manuf. Technol. (2024) 1–22.
[28] Jacimovic, Jacim, et al. "Net shape 3D printed NdFeB permanent magnet." arXiv preprint arXiv:1611.05332 (2016).
[29] J. Jacimovic, T. Christen, E. Dénervaud, Self-organized giant magnetic structures via additive manufacturing in NdFeB permanent magnets, Addit. Manuf. 34 (2020) 101288.
[30] S. Li, et al., 3D printing of ductile equiatomic Fe-Co alloy for soft magnetic applications, Addit. Manuf. 47 (2021) 102291.
[31] Nakajima, K., et al. "Additive Manufacturing of Magnetostrictive Fe–Co Alloys. Materials 2022, 15, 709." (2022).
[32] S. Pramanik, et al., Investigating the microstructure of an additively manufactured FeCo alloy: an electron microscopy study, Addit. Manuf. 46 (2021) 102087.
[33] D.M. Smith, Additive Manufacturing of Iron-Cobalt Alloy for Electric Motors, University of Dayton, 2021. MS thesis.
[34] A.B. Kustas, et al., Characterization of the Fe-Co-1.5 V soft ferromagnetic alloy processed by Laser Engineered Net Shaping (LENS), Addit. Manuf. 21 (2018) 41–52.
[35] Y. Zhang, et al., Microstructures and magnetic properties of Fe-35% Co alloy fabricated by metal injection molding, J. Magn. Magn. Mater. 497 (2020) 165982.
[36] L. Henderson, et al., Altering magnetic properties of iron filament PLA using magnetic field assisted additive manufacturing (MFAAM), J. Magn. Magn. Mater. 538 (2021) 168320.
[37] P. Afshari, et al., Mechanical strain tailoring via magnetic field assisted 3D printing of iron particles embedded polymer nanocomposites, Macromol. Mater. Eng. 308 (11) (2023) 2300194.
[38] A. Sarkar, M. Parans Paranthaman, I.C. Nlebedim, In-situ magnetic alignment model for additive manufacturing of anisotropic bonded magnets, Addit. Manuf. 46 (2021) 102096.
[39] Lu. Lu, P. Guo, Y. Pan, Magnetic-field-assisted projection stereolithography for three-dimensional printing of smart structures, J. Manuf. Sci. Eng. 139 (7) (2017) 071008.
[40] Koyalamudi, Kiran Babu, Ruoyu Yang, and Rahul Rai. "Additive Manufacturing of Conductive Polymer Nanocomposites Under the Influence of External Magnetic Field." International Design Engineering Technical Conferences and Computers

and Information in Engineering Conference. Vol. 50077. American Society of Mechanical Engineers, 2016.
[41] Y. Hu, R. Giesa, H.W. Schmidt, Recent progress in field-assisted additive manufacturing: materials, methodologies, and applications, Mater. Horiz. 8 (3) (2021) 748–769.
[42] A. Al Noman, B.K. Kumar, T. Dickens, Field assisted additive manufacturing for polymers and metals: materials and methods, Virtual and Physical Prototyping 18 (1) (2023) e2256707.
[43] R. Zhao, C. Chen, S. Shuai, T. Hu, Y. Fautrelle, H. Liao, Z. Ren, Enhanced mechanical properties of Ti6Al4V alloy fabricated by laser additive manufacturing under static magnetic field, Materials Research Letters 10 (8) (2022) 530–538.
[44] H. Zhou, C. Song, Y. Yang, C. Han, M. Wang, Y. Xiao, Z. Liu, The microstructure and properties evolution of SS316L fabricated by magnetic field-assisted laser powder bed fusion, Mater. Sci. Eng. A 845 (2022) 143216.
[45] G. Li, Z. Wang, L. Yao, D. Xie, G. Chen, Concentration mixing and melt pool solidification behavior during the magnetic field assisted laser cladding of Fe-Cr-based alloy on 45 steel surface, Surf. Coat. Technol. 445 (2022) 128732.
[46] Wang, J., Wang, Y., Shi, J., & Su, Y. (2019, November). Effect of external magnetic field on the microstructure of 316L stainless steel fabricated by directed energy deposition. In ASME International Mechanical Engineering Congress and Exposition (Vol. 59384, p. V02BT02A035). American Society of Mechanical Engineers.
[47] Y. Wang, X. Chen, Q. Shen, C. Su, Y. Zhang, S. Jayalakshmi, R.A. Singh, Effect of magnetic Field on the microstructure and mechanical properties of inconel 625 superalloy fabricated by wire arc additive manufacturing, J. Manuf. Process. 64 (2021) 10–19.
[48] P.Y. Wu, M. Hirtler, M. Bambach, H. Yamaguchi, Effects of build-and scan-directions on magnetic field-assisted finishing of 316L stainless steel disks produced with selective laser melting, CIRP J. Manuf. Sci. Technol. 31 (2020) 583–594.
[49] W. Zhao, Y. Wei, X. Zhang, J. Chen, W. Ou, Comparative investigation of wire arc additive manufacturing of Al-5% Mg alloy with and without external alternating magnetic field, Int. J. Adv. Manuf. Technol. (2022) 1–17.
[50] Celotta, R. J., et al. "Techniques to measure magnetic domain structures." Methods in Materials Research: Current Protocols (1999).